Self-Assembly Behavior and Doxorubicin-Loading Capacity of Acylated Carboxymethyl Chitosans

Kun-Ho Liu, Bo-Rong Chen, San-Yuan Chen, and Dean-Mo Liu*

Department of Materials Science and Engineering, National Chiao Tung University, 1001 Ta-hsueh Road Hsinchu, Taiwan, Republic of China

Received: March 9, 2009; Revised Manuscript Received: May 17, 2009

A new type of acylated carboxymethyl amphiphilic chitosan (ACC) with the use of acyl chain of varying lengths, from C_2 to C_{12}, and various degrees of acyl substitution was successfully synthesized and has been characterized in terms of its self-assembly behavior, structural stability, and drug encapsulation. The resulting nanostructure of the ACC nanoaggregates can be well manipulated through a control of hydrophobicity. Structural evolution of the self-assembled nanoaggregates is extensively characterized via ^{1}H NMR, FTIR, DSC, and TEM. A critical value of the hydrophobic effect, ($X_{DH} \times X_{Cn}$), i.e., a product of "degree of acyl substitution" and "carbon number of acyl chain", can be employed as an indicator for structural variation of the nanoaggregates: when ($X_{DH} \times X_{Cn}$) exceeded 1.5, the architecture of the nanoaggregates underwent a structural transformation from solid nanoparticle to hollow nanocapsules. The nanoaggregates exhibited an excellent colloidal and structural stability in aqueous medium. An improved affinity toward drug encapsulation, i.e., doxorubicin, can be technically designed according to the amphiphilic nature of the resulting nanoaggregates for drug delivery.

1. Introduction

The construction of supramolecular assemblies with well-defined nanostructure is of great interest owing to their potential applications in diverse fields. Since 1995 when Eisenberg et al.[1] found the multiple morphologies of crew-cut micelle-like aggregates of polystyrene-b-poly (acrylic acid) diblock copolymer in solution, the preparation and assembly of amphiphatic polymers of various architectures has become a research area of interest.[2] Polymer amphiphiles enable the preparation of nanoaggregates with shape ranging from spheres[3] to cylinders,[4] vesicles,[5] donuts,[6] and other geometries[7] by self-assembly. Of the various aggregates, hollow vesicles represent an important class of materials because their unique structural and surface properties may lead to a wide range of applications, especially in medicine such as capsule agents for drug delivery,[8] encapsulation of large quantities of guest molecules, and gene therapy.[9]

Recently, many efforts have been performed to prepare biodegradable and nontoxic polymeric amphiphatic on the basis of natural biomaterials such as polysaccharides. Among those natural biopolymers, hydrophilically,[10] hydrophobically,[11] and amphiphatically[12] modified chitosan derivatives were studied and realized to form monodisperse self-aggregated nanoparticles by ultrasonication in aqueous solutions. To further stabilize the self-aggregates, much effort has been placed in searching for cross-linkers upon forming a physically and chemically stable aggregate. However, the use of a clinically desirable cross-linker for the resulting chitosan-based aggregates more accessible to the field of drug delivery or medicine has been limited to those of nontoxic, biocompatible, and biodegradable agents. On this basis, a shift from conventional toxic cross-link agents such as glutaraldehyde,[13] sulfuric acid,[14] epoxy compounds,[15] and dialdehyde[16] to natural extractions such as genipin and quinine[17] has been elucidated in some detail and has received a great deal of attentions. Amphiphilic chitosan derivatives, after self-assembling into nanocapsule architecture as a result of intermolecular and/or intramolecular hydrophobic interactions, form a core phase where hydrophobic segments reside, while the hydrophilic segments forming the outer structure are exposed to the aqueous environment, resulting in a lowest-free-energy interface with the environment. Hence, either hydrophobically or amphiphilically modified chitosan derivatives are being produced to form the dispersed self-aggregated nanoparticles by ultrasonication in aqueous media due to noncovalent association arising from intra- or/and intermolecular interactions among hydrophobic segments in aqueous media.

However, it is more technologically desirable and critical if (a) a hollow structure can be easily achieved using chitosan derivatives without the need of extensive ultrasonication, where a nanometric carrier with higher load capacity of drugs or proteins can be expected with lower operation cost, (b) a variation of the amphiphilic nature of the resulting carrier allows an enhanced affinity to different drugs or proteins, e.g., hydrophilic drugs or hydrophobic drugs, where an improved encapsulation efficiency can be designed, (c) an adjustable biocompatibility and biodegradability is clinically manageable, and (d) a cross-linker-free but structurally stable colloid upon self-aggregation, after extensive dilution, can be obtained. In our previous work,[18] a simple core-template-free strategy was successfully proposed, and a new type of amphiphatic chitosan hollow nanocapsule was synthesized by a self-assembly mechanism. In general, polymer amphiphiles consisting of hydrophilic and hydrophobic segments can form micelles or micelle-like self-assemblies with a hydrophobic core and a hydrophilic shell due to noncovalent association arising from intra- and/or intermolecular interactions among hydrophobic segments in aqueous media.[19] On the other hand, the hollow cavity enclosed by a double layer membrane was also evolved as increasing the degree of hydrophobic substitution.[18]

* Corresponding author. Tel.: +886-3-5712121ext. 55391. Fax: +886-3-5725490. E-mail: deanmo_liu@yahoo.ca.

10.1021/jp902103p CCC: $40.75
Published on Web 08/13/2009

TABLE 1: Preparation Conditions and Characteristics of ACC Nanoaggregates

samples	acyl group	DH[a] ± 0.03	$[(RCO)_2O]/[GlcN]$	temp (°C)/time (h)	CAC[b] × 10^{-2} (mg/mL)	$W_{nf,max}$[c] (%)
CC	−	0	−	−	25.0	10.3
C_2−0.125	acetyl	0.11	0.2	25/20	21.0	11.8
C_2−0.25	acetyl	0.24	0.4	25/20	12.7	14.5
C_2−0.325	acetyl	0.31	0.5	25/20	7.20	15.9
C_2−0.5	acetyl	0.56	1	25/20	5.00	17.9
C_6−0.125	hexanoyl	0.13	0.2	25/20	9.20	12.4
C_6−0.25	hexanoyl	0.26	0.4	25/20	31.7	19.8
C_6−0.325	hexanoyl	0.33	0.5	25/20	0.91	24.8
C_6−0.5	hexanoyl	0.48	1	25/20	0.40	29.3
C_{10}−0.125	decanoyl	0.12	0.2	25/20	6.20	15
C_{10}−0.25	decanoyl	0.24	0.4	25/20	1.80	24.3
C_{10}−0.325	decanoyl	0.34	0.5	25/20	0.57	41.2
C_{10}−0.5	decanoyl	0.45	1	25/20	0.36	57.4
C_{12}−0.125	dodecanoyl	0.1	0.2	50/2 + 25/18	5.00	16.2
C_{12}−0.25	dodecanoyl	0.22	0.4	50/2 + 25/18	1.20	31.4
C_{12}−0.325	dodecanoyl	0.3	0.5	50/2 + 25/18	0.36	45.7
C_{12}−0.5	dodecanoyl	0.44	1	50/2 + 25/18	0.32	63.9

[a] DH determined by element analysis. [b] Critical aggregation concentration determined from I_{372}/I_{385} data. [c] The content of bound water obtained by the DSC test.

As the research objectives in the present study, self-assembled characteristics of the novel amphiphilic chitosan with various acyl lengths and its capability of drug encapsulation (with doxorubicin as a model molecule) will be systematically investigated in terms of different degrees of acyl substitution (DH) and carbon number of the acyl ligand (C_n), representing various degrees of hydrophobic interaction and its effect on morphological developmemt, colloidal stability, and drug affinity.

2. Experimental Section

2.1. Materials. Chitosan (M_w = 215 000 g·mol^{-1}, deacetylation degree = 85−90%) was supplied by Aldrich-Sigma. 2-Propanol, sodium hydroxide, chloroacetic acid, acetic anhydride, hexanol anhydride, decanoic anhydride, and dodecanoic anhydride purchased from Sigma Co., USA, were reagent grade. These materials were used as received in this investigation.

2.2. Synthesis of Chitosan Derivatives. ***2.2.1. Synthesis of Carboxymethyl Chitosan (CC).*** Following our previous report,[18] 5 g of chitosan was suspended in 2-propanol (50 mL) at room temperature while being stirred for 30 min. The resulting suspension was gently mixed with 12.5 mL of NaOH solution. The mixture containing NaOH of 13.3 M was mixed with 25 g of chloroacetic acid to prepare the CC sample with a high degree of carboxymethyl substitution. The resulting suspensions were stirred for 30 min and heated to 60 °C for 4 h, followed by filtration, washing by methanol solution, and drying. The degree of COOH substitutions was close to 0.50 measured by ^{1}H NMR.[18]

2.2.2. Synthesis of Acylated Carboxymethyl Chitosan (ACC). The obtained CC sample (2 g) was dissolved in distilled water (50 mL) under vigorous stirring for 24 h. These resulting solutions were then mixed with methanol (50 mL), followed by addition of acyl anhydrides, namely, acetic anhydride, hexanol anhydride, decanoic anhydride, and dodecanoic anhydride, representing acyl groups of various chain lengths (or carbon numbers). The acylated chitosan derivatives were prepared as previously described.[20] Acetyl, hexanoyl, and decanoyl carboxymethyl chitosan were prepared at ambient temperature for 20 h. Dodecanoic carboxymethyl chitosan was prepared at 50 °C for 2 h, followed by standing for 18 h. Different ratios of acyl anhydride to amino functionalities of CC samples were designed to prepare the ACC of different DH until the value of DH reached up to 0.5. The DH is defined as the average number of acyl groups per repeat unit multiplied by 100, calculated according to the nitrogen content which was determined by elemental analysis.[21] The degree of acylation was calculated using the following equation: DH = [(C/N − 5.48)/5.14]. Finally, the resulting solutions were collected by a dialysis membrane after dialysis with ethanol solution (25% v/v) for 24 h. The chemically modified chitosan was expressed using the values of n and m to define the carbon number of the hydrophobic side chain length (C_n) and DH, respectively, of the ACC derivative in the C_n−m, where n ranges from 2, 6, 10, to 12 and m ranges from 0.125, 0.25, 0.375, to 0.5. For example, C_2−0.25 means the ACC has the approximate value of the degree of hydrophobic substitution of 0.25. The preparation conditions and the characteristics of ACC samples are given in Table 1.

2.3. Preparation of ACC Nanoaggregates. ACC samples (100 mg/mL) were separately suspended in distilled water under gentle shaking at 25 °C for 24 h, followed by ultrasonication using a probe type sonifier (Automatic Ultrasonic Processor UH-500A, China) at 30 W for 2 min until an optically clear solution was obtained. The sample solutions were filtered through a filter (1.0 μm, Millipore) to remove dust and impurities. The final solutions were then stored in stock for a subsequent sample characterization.

2.4. Characterization. Proton nuclear magnetic resonance spectroscopy (^{1}H NMR) spectra were acquired to confirm the sites and degrees of substitution recorded by an NMR spectrometer (Varian unityinova 500) at 270 MHz. The samples were dissolved at a concentration of 10 mg/mL in D_2O, and the spectra were performed at 353 K. FTIR spectra were recorded with KBr pellets on a Bomem DA8.3 spectrometer (Canada) for tablet analysis in the spectral region (4000−400 cm^{-1}) with 64 scans recorded at a resolution of 4 cm^{-1}. For elemental analyses, samples were extensively dried (80 °C, 24 h) prior to submission of samples. Elemental analyses were performed with a Heraeus Vario III-NCH elemental analyzer (Germany).

The differential scanning calorimeter (DSC, Perkin-Elmer instrument) was employed to identify the content and structural configuration of water molecules in the ACC nanoaggregates while dispersing in aqueous solution.[22] The ACC solutions of 1.3% (w/v) were prepared by dissolving the obtained derivates in DI water. These suspensions were then cast onto Petri dishes

and dried at room temperature for 24 h, to form final dried samples. Those dried samples were later subjected to swelling in DI water with various time durations of 1, 2, 3, 4, and 5 min of swelling, respectively, corresponding to various amounts of water content. Samples were quenched from room temperature to 213 K and conditioned at 213 K for 10 min prior to the DSC test. DSC curves were then obtained by heating the sample to 300 K at a scanning rate of 10 K min^{-1}. The maximum content of nonfreezable bound water ($W_{nf,max}$) can be determined by detecting the endothermic peak assigned to the first-order phase transformation of water in the samples with various contents of water. The endothermic peak of freezable bound water is not detected until a critical amount of water is added to the sample. The critical amount of water is correlated with the number of tight water binding sites.

Nanostructure evaluation of the hollow nanocapsules was examined using transmission electron microscopy (TEM) (JEOL2100, Japan) and scanning electron microscopy (SEM) (JEOL-S6500, Japan). Sample solutions, diluted 10 times with the same aqueous solution, were dropped onto the carbon-coated 300 mesh copper grids and fast dried at 50 °C, then examined without being stained for TEM analysis. For SEM observation, the sample was dip-coated on the silicon substrate. The dried samples were further coated with gold (~20 nm thickness) for SEM analysis.

2.5. Self-Assembly Behavior of ACC. The pyrene solution (1.0×10^{-4} M) in methanol was added into the test tubes and evaporated under a stream of nitrogen gas to remove the solvents. Then, the solutions of ACC nanoaggregates were added into the test tubes. The final concentration of pyrene in a sample solution was 1.0×10^{-6} M, which was nearly equal to the solubility of pyrene in water at 22 °C.[23] The mixtures were sonicated for 30 min in an ultrasonic bath and shaken in a shaking air bath for 1 h at room temperature. Pyrene emission spectra were recorded on a fluorescence spectrophotometer (Hitachi, FL-4500, Japan). The probe was excited at 343 nm, and the emission spectra were recorded in the range of 350−500 nm at an integration time of 1.0 s. The excitation and emission slit openings were 10 and 2.5 nm, respectively.

2.6. Drug Loading Efficiency. Drug-loaded ACC nanoaggregates were prepared by dissolving doxorubicin (DOX) (20 μg/mL) in 20 mL of acquired suspension. Insoluble, free DOX was removed by centrifugation at 2000 rpm and 4 °C for 5 min. The drug-containing nanoparticles were then separated from the aqueous solution by centrifugation at 15 000 rpm and 4 °C for 15 min. Drug concentration in the supernatant was analyzed by ultraviolet absorption (UV) at a wavelength of 490 nm, a strong characteristic absorption band of DOX, with reference to a calibration curve on a UV−vis spectrometer (SP-8001, Metertech Inc.). The measurements were performed in triplicate. The amount of the drugs encapsulated in the nanoaggregates was then calculated by the total amount of DOX subtracting the residual DOX in the supernatant. Encapsulation efficiency (EE) was obtained as described below

$$EE = (A - B)/A \times 100$$

where A is the total amount of the DOX and B is the amount of DOX remaining in the supernatant.

3. Results and Discussion

3.1. Structural Characteristics of ACC. Scheme 1 schematically displays the molecular structure of the amphiphilically modified chitosan (ACC) synthesized using CC with different

SCHEME 1: Acylation Reaction of Carboxymethyl Chitosan

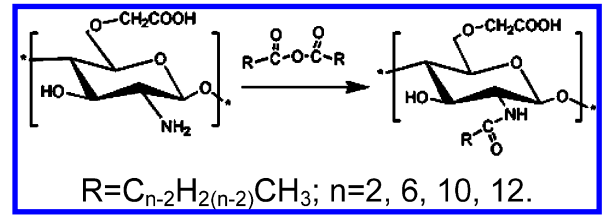

lengths of acyl side chains (with different carbon number, C_n, ranging from 2, 6, 10, to 12). In previous work, it was demonstrated that a hydrogen atom on the amino group of CC can be replaced by an acyl group, as confirmed by ^{1}H NMR analysis.[18] Figure 1 shows the ^{1}H NMR spectra of CC, C_2−0.125, C_6−0.125, and C_{12}−0.125. The proton assignment of CC (Figure 1(a)) is as follows (ppm): 2.06 (CH_3, acetamido group of chitosan), 3.22 (CH, carbon 2 of glucosamine ring), 3.6−4.0 (CH_2, carbon 3, 4, and 6 of glucosamine ring), 4.26 (CH_2, carboxymethyl group). After acylation, i.e., C_2−0.125 (Figure 1(b)), the chemical shifts at 1.1 ppm (CH_3) were assigned to the protons on the acetyl group. On the other hand, for C_6−0.125 (Figure 6(c)), the chemical shifts at 0.7 ppm (CH_3), 1.1 ppm ($C_\delta H2$), 1.2 ppm ($C_\gamma H2$), 1.5 ppm ($C_\beta H2$), and 2.2 ppm ($COC_\alpha H_2$) were assigned to the protons on the hexanoyl group. This demonstrates acetyl and/or hexanoyl substitution replaced some of the amino and hydroxyl sites of the *N*,*O*-carboxymethyl chitosan. The method for determining the degree of hydrophobic substitution has been described before,[18] and the result is given in Table 1, where the proton signals in the ^{1}H NMR spectrum confirmed the presence of acyl groups. However, as the $C_n \geq 10$ (i.e., C_{10} or C_{12}), the signal intensity of the characteristic acyl protons was not in proportion to the DH of the acyl groups, which suggested that acyl groups aggregated to form hydrophobic microdomains to minimize their interaction in D_2O, as shown in Figure 1(d). This trend in the ^{1}H NMR spectra was consistent with other polymeric amphiphiles that formed aggregates in the aqueous phase.[24] Therefore, the DH for the C_2 sample obtained from the ^{1}H NMR analysis showed similar data as compared with the results of elemental analysis. Hence, the DH of ACC samples was also determined by elemental analysis[21] described in the Experimental Section. The ACC samples with different levels of DH and C_n were prepared through the control of various ratios of acyl anhydride to the amino group of the CC, which is listed in Table 1. Figure 2 shows the FTIR spectra of CC and ACC, where the absorption peaks of CS at ca. 1655 cm^{-1} can be assigned to the carbonyl stretching of secondary amides (amide I band), at 1570 cm^{-1} to the N−H bending vibration of nonacylated 2-aminoglucose primary amines, and at 1555 cm^{-1} to the N−H bending vibrations of the amide II band.[21] The presence of both 2-aminoglucose and 2-acetamidoglucose repeat units was confirmed by bands at 1655, 1570, and 1555 cm^{-1}. After carboxymethylation, CC shows an absorption peak at ca. 1730 cm^{-1}, which was assigned to the carboxymethyl dimer (O═COH···O═COH). Compared to CC, the vibrational band of C_{10}−0.5 corresponding to primary amino groups at 1570 cm^{-1} disappeared, while prominent bands at 1555 cm^{-1} were observed. In addition, peaks at 2850−2950 cm^{-1} ascribed to $-CH_2$ with their absorption intensity were proportional to the acyl chain length.[25] These results further confirmed a successful acyl substitution on the carboxymethyl chitosan and have been clearly substantiated using the NMR analysis mentioned above.

After dispersing in water followed by ultrasonication, the ACC conjugates formed self-assembled aggregates by hydro-

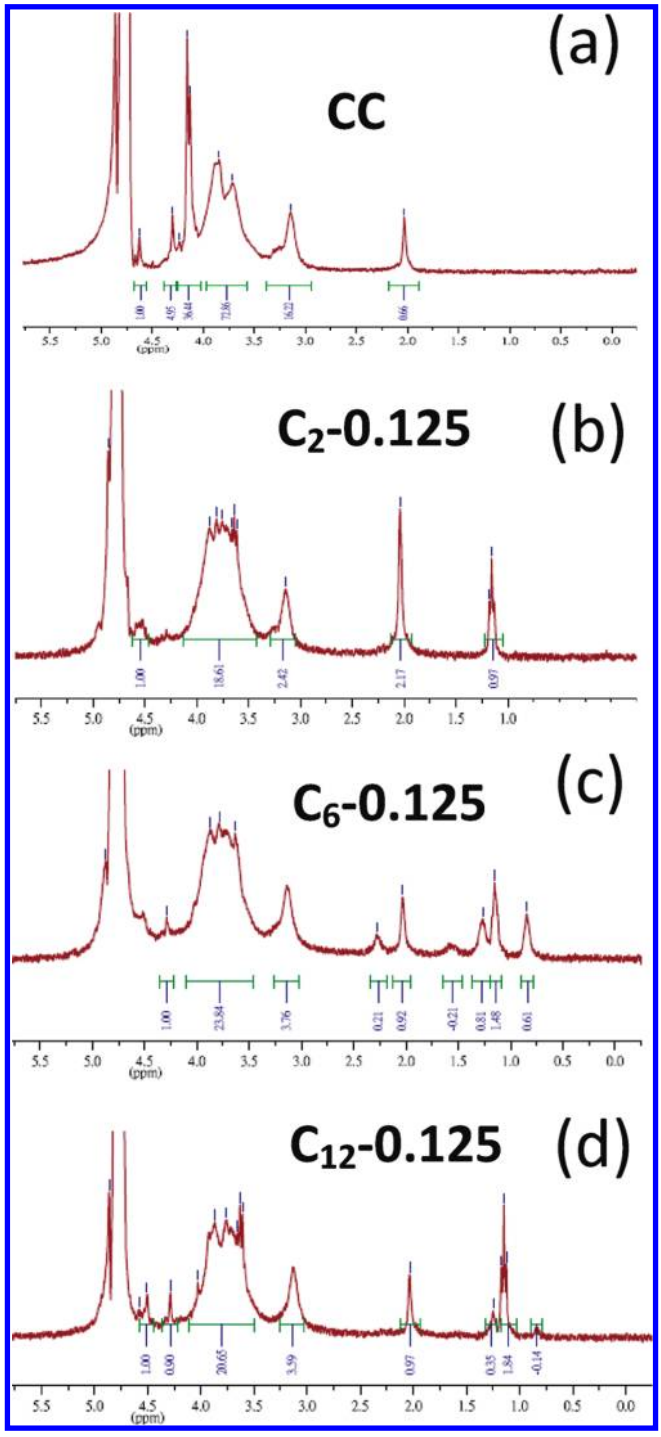

Figure 1. ^{1}H NMR spectrum of (a) CC, (b) $C_2-0.125$, (c) $C_6-0.125$, and (d) $C_{12}-0.125$.

phobic interaction between hydrophobic side chains. The mean size of the ACC nanoaggregates exhibits two different groups: one corresponds to a smaller size of around 20 nm, and the other is around 100 nm.[18] From TEM results [see Supporting Information, Figures S1 and S2], the ACC with lower hydrophobicity, i.e., the ACC with $C_n = 2$ and DH = 0.5, showed a compact particle morphology with a relatively uniform size distribution of around 25 nm in diameter. In addition, a structural change from particle to hollow capsule of larger particle size with increasing hydrophobicity, i.e., the ACC with $C_n = 6$ and DH = 0.5, was demonstrated before.[18] According to the poly core model proposed by Wang et al.,[26] the amphiphatic potential drives the resulting ACC macromolecules to self-assemble into

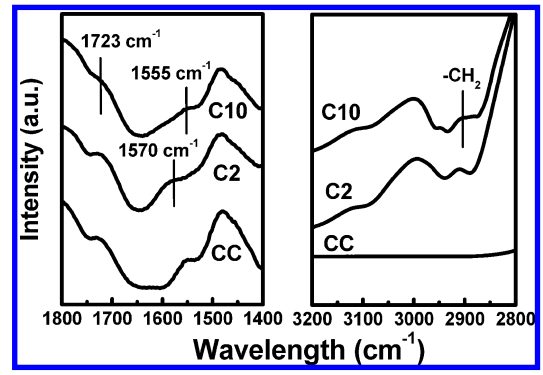

Figure 2. FTIR spectra of CC, $C_2-0.5$, and $C_{12}-0.5$.

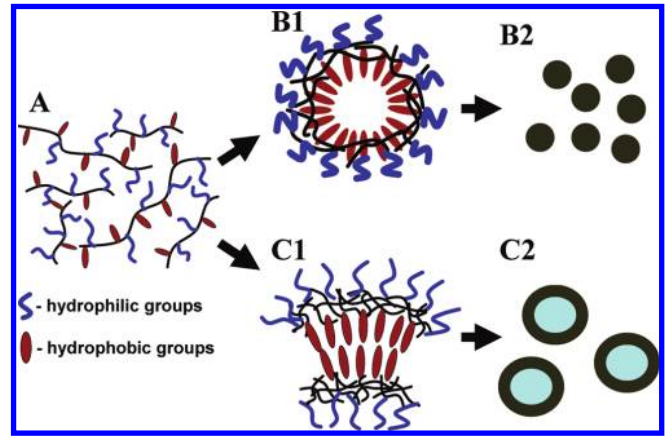

Figure 3. Schematic illustration of the formation process of ACC nanoaggregates.

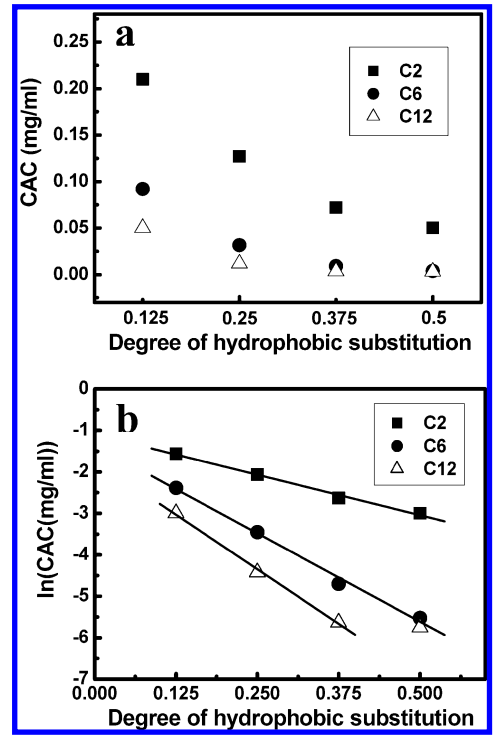

Figure 4. Dependence between the DH of ACC as $C_n = 2$, 6, and 12 and (a) the critical aggregation concentration CAC and (b) ln(CAC), respectively.

a micelle-like structure with hydrophobic groups turning into the core structure, while the hydrophilic segments structurally turn into the water environment to establish a shell structure, as schematically illustrated in the reaction scheme of A → B1

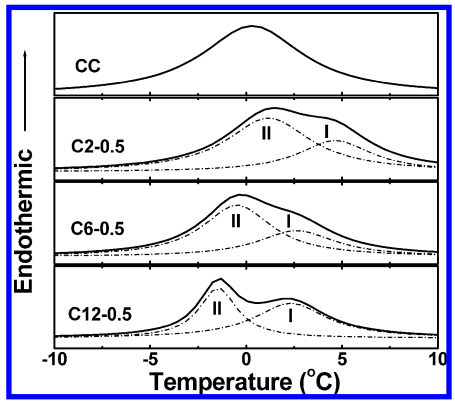

Figure 5. DSC curves of CC and ACC derivates (C_n−0.5) measured at a water content of 200%. Dashed lines represent the curve fitting by the Lorentzian curve-fitting procedure.

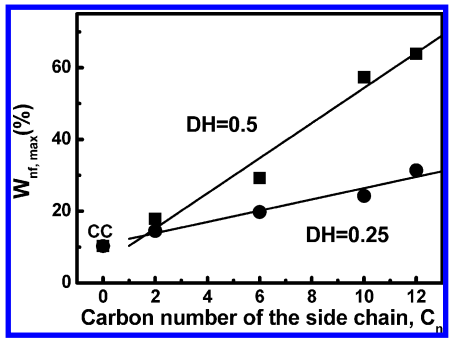

Figure 6. Dependence between the content of bound water, $W_{nf,max}$, and the hydrophobic side chain with different C_n of ACC in DH = 0.25 and 0.5.

in Figure 3, forming a spherical architecture with minimal surface energy (as shown in the drawing of B2 in Figure 3). In contrast, with an increase of free energy caused by increasing hydrophobicity, the ACC tends to self-aggregate to form a multilayer structure with a hydrophilic inner layer−hydrophobic intermediate layer−hydrophilic outer layer configuration as illustrated in the reaction scheme of A → C1 → C2 of Figure 3 where a capsule-like structure can be developed. Accordingly, the structural change from particle to hollow capsule is attributed to the different results of the self-assembly and physical state of water molecules within the aggregates caused by various degrees of hydrophobicity of ACC.

3.2. Self-Assembly Behavior of ACC. The fluorescence probe technique can be used to monitor the self-aggregation behavior of ACC at a molecular level, and pyrene was chosen as a fluorescence probe.[27] The intensity ratio of the first peak (372 nm) and the third peak (385 nm) I_{372}/I_{385} in its fluorescent spectrum is quite sensitive to a subtle change in the environment around the pyrene molecules. Hence, the critical aggregation concentration (CAC), which is defined as the threshold concentration of self-aggregate formation by intra- and/or intermolecular interactions, can be determined from the variation of the I_{372}/I_{385} value of pyrene in the presence of polymeric amphiphiles, as listed in Table 1. Figure 4a shows the change of CAC of ACC nanoaggregates with different levels of DH and C_n. It was found that the CAC of ACC with DH and C_n varying from 0.125 to 0.5 and from 2 to 12, respectively, has a smaller value than that of the CC (which was 0.25 mg/mL as previously reported[18]), indicating that the ACC possesses stronger self-aggregation behavior than that of CC in aqueous solutions. This stronger tendency of the self-aggregation can be deduced from the increased hydrophobicity caused by the introduction of greater DH and C_n. In addition, it is also observed that the CAC values of ACC nanoaggregates were decreased with the increase of DH and/or C_n. It has realized that the increase of hydrophobicity in amphiphatic polymer causes the difficulty to dissolve in aqueous solution because the energy is essential to dissociate the H-bonding in water molecules (need to do work). Therefore, the dissolution of hydrophobic groups in water will give rise to an increase of the surface free energy. To reduce the energy, the hydrophobic groups will aggregate to form a micelle-like structure with a hydrophobic core and a hydrophilic shell or a multilayer configuration. Hence, with larger DH and/or C_n, the ACC is able to form nanoaggregates easily at very low concentrations because it tends to reach the largest surface energy. This demonstrates that the self-aggregation ability can be effectively enhanced with increasing hydrophobic nature, e.g., DH and/or C_n, of the ACC in aqueous environment. However, it seems to have the lowest value of CAC even if the DH or/and C_n is infinitely increased. This means that the CAC of the ACC nanoaggregates will reach a lowest value over a critical level of hydrophobicity. In addition, a linear correlation between ln(CAC) and DH was observed, except the case when C_n is 12 and DH is 0.5, as shown in Figure 4b. The same linear correlation between ln(CAC) and C_n can be also obtained. Such a linear correlation proves that the CAC of the ACC nanoaggregates decreased exponentially with the increase of DH and C_n. Hence, a mathematical relationship among ln(CAC), DH, and C_n can be derived as follows

$$\ln(\mathrm{CAC}) = a_1 X_{C_n} \cdot X_{\mathrm{DH}} + b_1 X_{\mathrm{DH}} + c_1 X_{C_n} + d_1 \quad \text{at } X_{\mathrm{DH}} < 0.5,\ X_{C_n} < 12 \qquad (1)$$

or

$$\mathrm{CAC} = \exp[a_1 X_{C_n} \cdot X_{\mathrm{DH}} + b_1 X_{\mathrm{DH}} + c_1 X_{C_n} + d_1] \quad \text{at } X_{\mathrm{DH}} < 0.5,\ X_{C_n} < 12 \qquad (2)$$

where the coefficients, i.e., a_1, b_1, c_1, and d_1, having the values of 0.24, −6.87, −0.21, and −0.38, respectively, were obtained by regression analysis. From eq 2, it can be suggested that from the hydrophobic effect resulting from both the DH and side chain length C_n dominates the self-aggregation ability of the ACC nanoaggregates. Compared to the case of C_2, the slopes were apparently increased for the cases of C_6 and C_{12} in the semilog plot (Figure 4b), indicating that a potentially stronger hydrophobic effect can be developed through a longer-chain acyl substitution, where a much lower value of CAC, by 2−3 orders of magnitude, can be obtained.

3.3. Molecular Configuration of Water in ACC. The hydrophobic substitution is also found to affect profoundly water uptake behavior of the resulting ACC. It was generally accepted that the hydrophobic modification of amphiphatic chitosan derivatives with various chain lengths may cause a change in the molecular configuration of water that is trapped in the matrix. To better understand the physical state of water molecules that are trapped in the ACC network, DSC analysis was conducted. Accordingly, the configuration of the water molecules, corresponding to the resulting DSC spectrum, can be classified into three different physical states:[28] (1) free water which can freeze at the usual freezing point (corresponding to an endothermic peak close to 4.8 °C), (2) freezable bound water which freezes at a temperature lower than the usual freezing point (corresponding to an endothermic peak much lower than 4.8 °C), and

(3) nonfreezable bound water which cannot freeze at the usual freezing point (which is hardly detected by the DSC).

In the initial swelling process, water molecules first disrupt the intermolecular hydrogen bonds and then bind to the hydrophilic sites, such as carboxymethyl groups in this case. These water molecules, which are isolated and uniformly distributed throughout the polymer, have greatly restricted mobility and are referred to as nonfreezable bound water. Above a certain level of the bound water, the additional water is preferentially oriented around the bound water and the polymer network structure as a secondary or tertiary hydration shell, which is in a form generally called "clusters". These cagelike structures result from the tendency of water molecules to form the maximum amount of hydrogen bonds among them in the available space. This type of water is called freezable bound water. As the water uptake further increases, the splitting of the melting peak will becomes more apparent in the DSC curves, suggesting the existence of two states of freezing water, i.e., freezable bound water and free water, in the polymers. Figure 5 shows the DSC spectra of the samples with different chain length of acyl groups measured at water content of about 200%. A heavily overlapped band (solid line) is observed and can be clearly differentiated as an overlap of several peaks (depicted as dash lines) using the Lorentzian curve-fitting procedure. For the CC sample, the endothermic peak of free water was not observed under a fully swollen state. Instead, the endothermic peaks at 1.3 °C and below assigned to freezable bound water were detected. However, after acyl modification, the samples show different DSC spectra, suggesting the state of water in the ACC network was significantly different from that in the CC. It can be found that the peak I which is close to 4.8 °C suggests that the ACC contained free water when the water content ≥200%. On the other hand, the peak II was assigned to freezable bound water. With an increase of the side chain length from $C_n = 2$ to 12, peaks I and II shifted toward lower temperature, and the peak intensity was decreased, which may be caused by the decrease of the intermolecular volume for free water and freezable bound water. This implies that the chain length of the acyl group plays an important role in affecting the amount of free water and freezable bound water within the network structure.

Hence, to understand the interaction between water molecules and the hydrophobic side chain of the ACC, DSC is also used to quantitatively determine the amount of water, i.e., both freezable and nonfreezable bound water in the ACC matrix. Figure 6 shows the $W_{nf,max}$ in ACC with different C_n. It was found that the CC displays the lowest $W_{nf,max}$ of 10.3% than other samples. This is due to the fact that the samples with high carboxymethyl substitution favored the formation of intermolecular hydrogen bonding (polymer−polymer interaction), resulting in a structure with fewer tight water-binding sites (water−polymer interactions).[29] However, with the increase of the hydrophobic side chain length, the $W_{nf,max}$ of ACC is proportionally increased with the C_n until $C_n = 12$. This C_n-dependent increment can be attributed to a so-called "hydrophobic effect" under which water becomes more structured and less mobile in the vicinity of the hydrophobic group.[30] It has been known from surface-thermodynamic analyses that the attractive interactions between apolar (hydrophobic) molecules immersed in water are driven by the strong hydrogen-bonding free energy of cohesion between the surrounding water molecules.[31] Hence, increasing the C_n of the side chain will cause an increase of the hydrophobizing capacity of water since it tends to increase the tendency of self-hydrogen-bonding among water molecules, rather than the interactions between the water molecule and the host molecule. Differing from the CC (which has a stronger water−polymer interaction), the hydrophobic interaction between acyl groups is suggested to cause more self-hydrogen-bonding for those neighboring water molecules. The strong hydrophobic effect coming from the hydrophobic substitution will enhance the hydrophobizing capacity of water, and this behavior is increased with increasing hydrophobicity of the ACC as the acyl chain length increased (i.e., larger C_n).

On this basis, a linear correlation between $W_{nf,max}$ of the ACC and the C_n with DH of 0.5 and 0.25 is then revealed as depicted in Figure 6, which provides direct evidence that the content of bound water in the ACC is profoundly dependent on the hydrophobic side chain length. Moreover, the slope of these curve-fitting straight lines is increased linearly with the increase of DH. The linearity correlation suggests the "bound water" is affected linearly with both the DH and C_n, and accordingly, linear mathematical equations can be derived directly from the experimental data, which is given as follows

$$Y_w = (11.87 \cdot X_{DH} - 1.2) \cdot X_{Cn} + K_1 \quad (3)$$

and

$$Y_w = (11.22 \cdot X_{Cn} - 3.16) \cdot X_{DH} + K_2 \quad (4)$$

where Y_w is the concentration of bound water; X_{DH} is the degree of hydrophobic substitution; X_{Cn} is the carbon number; and K_1 and K_2 are constant.

By further integration of eqs 3 and 4, a mathematical model can be constructed as follows

$$Y_w = a_2 X_{Cn} \cdot X_{DH} + b_2 X_{DH} + c_2 X_{Cn} + d_2 \quad \text{at } X_{DH} < 0.5, X_{Cn} < 12 \quad (5)$$

The coefficients a_2, b_2, c_2, and d_2, having values of 11.9, −13.8, −1.20, and 13.1, respectively, were obtained by regression analysis. This new model, having exactly the same as eq 1, indicates that the bound water is a complex function of C_n and DH. To be more specific, the bound water is influenced adversely by X_{DH} and X_{Cn} alone but more significantly by the term of $(X_{DH} \times X_{Cn})$. The latter implies that the concentration of bound water trapped within this newly formed ACC is profoundly influenced by a composite effect of DH and side chain length. Comparing to eq 1 and 5, it is believed that the self-aggregation behavior should be physically correlated with the content of bound water within the resulting ACC aggregates, and the composite effect as a result of both the degree of acyl substitution and chain length aforementioned should play an important role in determining the self-assembly behavior of the ACC molecules.

3.4. Self-Assembly Map. On this basis, an interesting finding can be drawn from Figure 7, showing the plot of CAC and $W_{nf,max}$ of ACC with different values of $(X_{DH} \times X_{Cn})$, where an intercept at product of $(X_{DH} \times X_{Cn}) = 1.5$ was observed. Below 1.5, assigned as Zone I, the values of CAC decreased readily with increasing $(X_{DH} \times X_{Cn})$ up to 1.5 and reached a minimum value. The content of bound water, $W_{nf,max}$, in the ACC was increased only slightly in the region of Zone 1. However, when the value of $(X_{DH} \times X_{Cn})$ exceeded 1.5 (i.e., Zone II), $W_{nf,max}$ increased considerably to a level as high as 64% with an increase of $(X_{DH} \times X_{Cn})$, while the CAC kept relatively constant. These

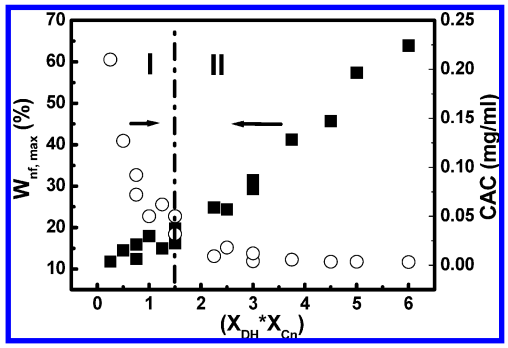

Figure 7. Plot of CAC (○) and $W_{nf,max}$ (■) of ACC derivates with different values of ($X_{DH} \times X_{Cn}$).

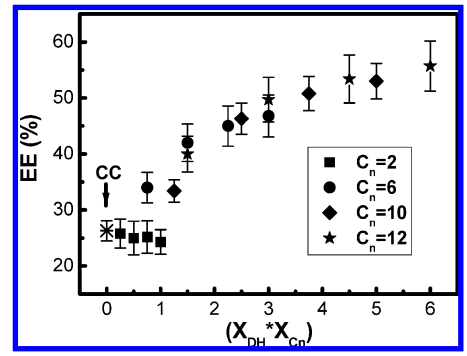

Figure 8. DOX encapsulation efficiency of ACC nanoaggregates with various values of ($X_{DH} \times X_{Cn}$).

findings strongly indicate that the hydrophobic effect was dominated by an interaction of both DH and C_n, rather than the individual component alone. Further, the hydrophobicity associated with DH and C_n strongly affected the self-aggregation ability and the hydrophobizing water capacity of the ACC nanoaggregates. It is clearly demonstrated that a critical level of hydrophobicity that can effectively generate conspicuous changes in both CAC and $W_{nf,max}$ is evidenced in the self-assembly map constructed in Figure 7, when the composite effect of the degree of acyl substitution and acyl chain length, i.e., the product of ($X_{DH} \times X_{Cn}$), is close to 1.5.

Upon self-assembly, the hydrophobicity of the ACC was detected to fatefully dominate the structural evolution of the nanoaggregates. Therefore, it is reasonable to believe from eqs 1 and 5, and together with Figure 7, that the composite effect between the DH and C_n may play a key role in controlling the structural morphology of the resulting nanoaggregates. In Zone I of Figure 7 (the region where the value of ($X_{DH} \times X_{Cn}$) is lower than 1.5), the nanoaggregates with $C_n = 2$ and DH = 0.5 showed a compact particle morphology [see Supporting Information, Figure S1]. This observation is similar to the case of the CC in previous work.[18] However, when ($X_{DH} \times X_{Cn}$) exceeded 1.5, i.e., Zone II, the resulting nanoaggregates exhibited an entirely different structural morphology. In the case of $C_n = 6$ and DH = 0.5, the ACC nanoaggregates show a perfect spherical geometry [see Supporting Information, Figure S2].

From a series of experimental observations, a hollow structure exists only when the term of ($X_{DH} \times X_{Cn}$) ≥ 1.5. As revealed from the fluorescence probe test, the CAC values for the nanoaggregates with a smaller range of ($X_{DH} \times X_{Cn}$) decreased rapidly until ($X_{DH} \times X_{Cn}$) approached 1.5. As aforementioned, the hydrophobizing water capacity of the nanoaggregates increased rapidly as a result of increasing hydrophobicity in the Zone II region. However, this would further cause structural instability when dispersed in aqueous solution due to the formation of an uncompatibilized interface between the aqueous phase and hydrophobic compartments of the ACC. Therefore, from the energetic viewpoint, the ACC with higher hydrophobic nature, i.e., the compositions underlying the region of Zone II, prefers to self-aggregate into a more thermodynamically stable form as such that the multilayer sandwich structure can be expected, where a capsule-like structure can be developed. On this basis, the ACC nanocapsules with hydrophilic segments residing in the outer and inner regions of the capsules ensure a thermodynamic and colloidal stability in aqueous solutions, and this is evidenced from a stability test where the nanocapsules were well dispersed in an aqueous solution (PBS at pH = 7.4) for a time period of as long as 30 days.

3.5. Doxorubicin Loading. The drug-loading capacity of the ACC nanoaggregates was carried out using DOX, a clinically important anticancer drug, as a model molecule. Since the DOX molecule contains an amino group with a pK_a of 8.6, it is expected that DOX is able to form a polyelectrolyte complex with the carboxymethyl groups of the ACC because of electrostatic attraction.[32] However, in our previous work,[18] an initial rapid release caused by free diffusion of DOX from the surface of nanocapsules out of the dialysis membrane was observed, and the encapsulation efficiency was fairly moderate. With the incorporation of hydrophobic ligands of varying size and substitution, Figure 8 gives the correlation between the DOX encapsulation efficiency (EE) in the ACC nanoaggregates and different values of ($X_{DH} \times X_{Cn}$). For CC, it showed only 26.3% EE due to the physical interaction between DOX molecules and carobxymethyl groups, as demonstrated in previous work.[18] After acyl modification (where $C_n = 2$), DOX encapsulation efficiency of the ACC nanoaggregates was slightly reduced from 26.3% to 24.5% with an increase of DH from 0 to 0.5. This decrease of EE is due to a decrease in the population of the functional group, i.e., carboxymethyl groups, along the ACC chains. This is further evidenced from Figure 2 where the intensity of the characteristic peaks at 1730 cm^{-1} is reduced, indicating a reduction of intermolecular interaction between carboxymethyl dimers as the C_n was increased. However, the EE of the ACC nanoaggregates for the DOX is increased considerably with the composite effect of both acyl chain length, i.e., $C_n = 6$, 10, and 12, and the degree of acyl substitution, to a value of about 56%. This finding clearly suggests a considerable improvement in chemical and/or physical affinity between the nanoaggregates (or nanocapsules) and the DOX, thus resulting in an enhancement of drug load efficiency by more than 200% compared to that of the CC composition. However, it should be noted that optimal encapsulation efficiency has not yet practiced for the ACC through other processing skills in this study; instead, the current experimental outcomes of the EE are simply illustrating the power of the hydrophobic nature and a successful design of hydrophobic interactions, i.e., the effect of ($X_{DH} \times X_{Cn}$), of the ACC nanoaggregates that can be used as an indicator for better drug loading manipulation.

4. Conclusion

A new type of ACC with a diverse character of self-assembly behavior has been systematically investigated through the use of varying degrees of DH and different C_n. Such a self-assembled ACC nanoaggregate displayed stable colloidal property at physiological pH for a long time period. Experimental observations also revealed that CAC and $W_{nf,max}$ of the ACC were strongly affected by both DH (symbolized as X_{DH}) and C_n

(as X_{Cn}), forming a strong composite effect. Evolution of the resulting self-aggregation structure of the ACC has been explored where a transformation from solid nanoparticle to hollow nanocapsule of the ACC was observed as a result of hydrophobic effect. A numerical model for such a composite effect, i.e., ($X_{DH} \times X_{Cn}$), on the hydrophobic effect has been experimentally proposed, which, together with drug load study, provides a technically useful indicator for improved loading efficiency for anticancer doxorubicin drug. More extensive analysis of the structure from molecular to nanometric scale in greater detail will be performed using more advanced techniques, including ^{13}C NMR, Cryo-TEM, small-angle neutron scattering (SANS), and/or small-angle X-ray scattering (SAXS), where we believe a much clearer picture of the structural evolution will be revealed and elucidated in a separated report.

Acknowledgment. This work was financially supported by the National Science Council of the Republic of China, Taiwan, under Contract No. NSC97-2627-B-009-006 and NSC98-2113-M-009-004.

Supporting Information Available: Figures S1 and S2. This material is available free of charge via the Internet at http://pubs.acs.org.

References and Notes

(1) Zhang, L.; Barlow, R. J.; Eisenberg, A. *Macromolecules* **1995**, *28*, 6055–6066.
(2) Won, Y. Y.; Davis, H. T.; Bates, F. S. *Science* **1999**, *283*, 960–963.
(3) Marencic, A. P.; Wu, M. W.; Register, R. A.; Chaikin, P. M. *Macromolecules* **2007**, *40*, 7299–7305.
(4) Gohy, J. F.; Lohmeijer, B. G. G.; Alexeev, A.; Wang, X. S.; Manners, I.; Winnik, M. A.; Schubert, U. S. *Chem.—Eur. J.* **2004**, *10*, 4315–4323.
(5) Rodriguez-Hernandez, J.; Lecommandoux, S. *J. Am. Chem. Soc.* **2005**, *127*, 2026–2027.
(6) Pochan, D. J.; Chen, Z. Y.; Cui, H. G.; Hales, K.; Qi, K.; Wooley, K. L. *Science* **2004**, *306*, 94–97.
(7) Cameron, N. S.; Corbierre, M. K.; Eisenberg, A. *Can. J. Chem.* **1999**, *77*, 1311–1326.
(8) Photos, P. J.; Bacakova, L.; Discher, B.; Bates, F. S.; Discher, D. E. *J. Controlled Release* **2003**, *90*, 323–334.
(9) Mishima, K. *Adv. Drug Delivery Rev.* **2008**, *60*, 411–432.
(10) Zhu, A.; Chan-Park, M. B.; Dai, S.; Li, L. *Colloids Surf. B: Biointerface* **2005**, *43*, 143–149.
(11) Chae, S. Y.; Son, S.; Lee, M.; Jang, M.-K.; Nah, J.-W. *J. Controlled Release* **2005**, *109*, 330–344.
(12) Suia, W.; Songa, G.; Chenb, G.; Xuc, G. *Colloid. Surf. A: Physicochem. Eng. Aspects* **2005**, *256*, 29–33.
(13) Goissis, G.; Junior, E. M.; Marcantonio, R. A. C.; Lai, R. C. C.; Cancian, D. C. J.; De Caevallho, W. M. Biocompatibility studies of anionic collagen membranes with different degree of glutaraldehyde cross-linking. *Biomaterials* **1999**, *20*, 27–34.
(14) Huang, R. Y. M.; Pal, R.; Moon, G. Y. Crosslinked chitosan composite membrane for the pervaporation dehydration of alcohol mixtures and enhancement of structural stability of chitosan/polysulfone composite membranes. *J. Membr. Sci.* **1999**, *160*, 17–30.
(15) Wei, Y. C.; Hudson, S. M.; Mayer, J. M.; Kaplan, D. L. The crosslinking of chitosan fibers. *J. Polym Sci. Part A: Polym Chem.* **1992**, *30*, 2187–2193.
(16) Schmidt, C. E.; Baier, J. M. Acellular vascular tissues: natural biomaterials for tissue repair and tissue engineering. *Biomaterials* **2000**, *21*, 2215–2231.
(17) (a) Mi, F. L.; Sung, H. W.; Shyu, S. S.; Su, C. C.; Peng, C. K. *Polymer* **2003**, *44*, 6521. (b) Jin, J.; Song, M.; Hourston, D. J. *Biomacromolecules* **2004**, *5*, 162. (c) Kuboe, K.; Tonegawa, H.; Ohkawa, K.; Yamamoto, H. *Biomacromolecules* **2004**, *5*, 348.
(18) Liu, K.-H.; Chen, S.-Y.; Liu, D.-M.; Liu, T.-Y. *Macromolecules* **2008**, *41*, 6511–6516.
(19) Rotureau, E.; Chassenieux, C.; Dellacherie, E.; Durand, A. *Macromol. Chem. Phys.* **2005**, *206*, 2038–2046.
(20) Seo, T.; Kanbara, T.; Iijima, T. *J. Appl. Polym. Sci.* **1988**, *36*, 1443–1451.
(21) Xu, J.; McCarthy, S. P.; Gross, R. A.; Kaplan, D. L. *Macromolecules* **1996**, *29*, 3436–3440.
(22) Agrawal, A. M.; Manek, R. V.; Kolling, W. M.; Neau, S. H. *J. Pharm. Sci.* **2004**, *93*, 1766–1779.
(23) Wilhelm, M.; Zhao, C.; Wang, Y.; Xu, R.; Winnik, M. A.; Mura, J. *Macromolecules* **1991**, *24*, 1033–1040.
(24) Park, K.; Kim, K.; Kwon, I. C. *Langmuir* **2004**, *20*, 11726–11731.
(25) Tien, C. L.; Lacroix, M.; Ispas-Szabo, P.; Mateescu, M.-A. *J. Controlled Release* **2003**, *93*, 1–13.
(26) Wang, Y.; Liu, L.; Weng, J.; Zhang, Q. *Carbohydr. Polym.* **2007**, *69*, 597–606.
(27) Amiji, M. M. *Carbohydr. Polym.* **1995**, *26*, 21–213.
(28) Guan, Y. L.; Shao, L.; Yao, K. D. *J. Appl. Polym. Sci.* **1996**, *61*, 2325–2335.
(29) Liu, T. Y.; Chen, S. Y.; Lin, Y. L.; Liu, D. M. *Langmuir* **2006**, *22*, 9740–9745.
(30) Tamai, Y.; Tanaka, H.; Nakanishi, K. *Macromolecules* **1996**, *29*, 6750–6760.
(31) van Oss, C. J.; Giese, R. F. J. *Disper. Sci. Technol.* **2004**, *25*, 631–655.
(32) Kitaeva, M. V.; Melik-Nubarov, N. S.; Menger, F. M. *Langmuir* **2004**, *20*, 6575–6579.

JP902103P